Strain-induced variant selection in heterogeneous nucleation of α-Ti at screw dislocations in β-Ti

Max Poschmann, Joseph Lin, Henry Geerlings, Ian S. Winter, and D. C. Chrzan

Phys. Rev. Materials **2**, 083606 — Published 24 August 2018

DOI: 10.1103/PhysRevMaterials.2.083606

Strain-Induced Variant Selection in Heterogeneous Nucleation of α-Ti at Screw Dislocations in β-Ti

Max Poschmann, Joseph Lin, Henry Geerlings, Ian S. Winter, and D. C. Chrzan

Department of Materials Science and Engineering,

*University of California, Berkeley, CA 94720, USA**

(Dated: August 2, 2018)

Abstract

Heterogeneous nucleation of the α to β phase transition at $\langle 1\ 1\ 1\rangle_\beta$-type screw dislocations in pure titanium is examined through a combination of elasticity theory and molecular dynamics simulation using a modified embedded atom method potential. These screw dislocations act as heterogeneous nucleation sites and increase the α phase growth rate, but also restrict the orientation of the α nuclei to certain directions along which the strain field of the dislocation aligns with the strain required to complete the Burgers transformation path. Simulations and elasticity theory predict the same three α phase variants along the same preferential directions for α nucleus growth in the early stages of transformation. Previous elasticity theory calculations indicate that this growth does not result in the elastically preferred habit plane for the α nucleus. Molecular dynamics simulations on many-layer supercells presented here show that large α plates will change their growth direction towards the predicted habit plane, but this rotation is resisted by the line tension of the dislocation until the α precipitate detaches from the dislocation.

I. INTRODUCTION

Titanium alloys are of obvious technological importance due to their often superior mechanical properties. These properties are engineered into the material through a variety of alloying additions and processing routes. A key aspect of this engineering is that Ti alloys have multiple phases accessible at room temperature - the α-phase (hexagonal close packed - hcp), the β-phase (body centered cubic - bcc) and the ω-phase (simple hexagonal). Alloy engineering often exploits these phase transitions (or seeks to suppress them) to improve alloy properties, and consequently the mechanisms by which the phase transformations occur are of interest.

Nucleated phase transitions offer the opportunity to influence the kinetics of the phase transformation. More specifically, first-order transitions can nucleate homogeneously within a (nominally) translationally invariant system and they can nucleate heterogeneously upon some defect within the transforming system, the latter of which is often overwhelmingly preferred. For example, suppression of heterogeneous nucleation sites for solidification can lead to substantial supercooling of liquids. Thus, understanding the heterogeneous nucleation paths available to the system can allow for control of a first-order phase transformation of interest. In pure Ti, the β to α phase transition is expected to proceed via the well-known Burgers path[1]. The Burgers path consists of both a strain and shuffling of atoms, described in more detail in Section IV. This path, however, involves overcoming an energy barrier, and hence the transition is first-order.

Due to the technological importance of α/β-Ti alloys, the α to β and β to α transitions in Ti have been studied extensively in experiment[2–11] as well as in phase field simulations[12–14]. The consensus among these previous studies is that the orientations of post-transformation α Ti grains are selected by the Burgers relation. Several of the studies which employed electron backscattering diffraction (EBSD) or X-ray diffraction further concluded that there is selection among the possible orientation variants resulting from the Burgers path[2–5]. In particular, Gey *et al.* have shown that increasing the degree of hot rolling in the β phase increases the degree of variant selection, and that the α variants preferentially selected are linked to the most active slip systems in the parent β grain[3]. Qiu *et al.* used anisotropic elasticity theory as well as phase field simulations to show that the stress fields around dislocations in the β phase interact with α nuclei, and that this elastic interaction dominates

the variant selection during nucleation[12].

Here we present atomistic simulations of the β to α transition around dislocations, with findings that are in good agreement with the preceding experimental and phase field work. In this paper, the influence of $\langle 1\ 1\ 1\rangle_\beta$-type screw dislocations on the β to α transition in pure Ti is studied using molecular dynamics (MD) employing an empirical potential. Specifically, dislocations are introduced into the β-phase at high temperatures. The system is then cooled to temperatures below the β to α phase transition temperature, and allowed to evolve. Given sufficient time, the system transforms to the α-phase. The simulations thus enable the dynamics of the transition to be studied in detail. Simulations are performed at several temperatures and the nucleation and growth rates calculated across the temperature range 1050 K to 1250 K. Below we show that the equilibrium $\alpha \rightarrow \beta$ transition temperature is approximately 1700 K. Hence these temperatures represent a substantial undercooling.

In the simulations, the α phase initially nucleates from the β phase as plates which have an edge terminated at a dislocation core. In the very initial stages of nucleation, the habit planes of these plates are determined by the stress field of the dislocations. However, as the nuclei grow, their habit plane shifts. Further, we find evidence of tent-like structures and 3-variant clusters as previously reported in experiment and phase field simulations[6,11,12]. These atomic scale simulations show that existing dislocation microstructures have the potential to alter dramatically the β to α transition kinetics and morphologies.

In the following, these results are presented in more detail. In Section II we introduce the various methods employed, including calculation of the β to α transition temperature by non-equilibrium thermodynamic integration. In Section III, we illustrate the predictions of our elasticity theory modelling and the results of our MD simulations of the β to α phase transition. Next we discuss the implications of these results within the context of the known Burgers path and elasticity theory in Section IV. Finally, the conclusions are presented.

II. METHODS

A. MEAM Potential Validation

Molecular dynamics calculations were performed using the Large-scale Atomic/Molecular Massively Parallel Simulator (LAMMPS)[15]. For our simulations of titanium, the modified

embedded atom method (MEAM) potential for titanium of Hennig *et al.*[16] was used. The titanium potential was analyzed to determine its β to α phase transition boundary. Using a non-equilibrium thermodynamic integration technique[17], the free energies of β- and α-phases can be calculated with small errors for a range of relevant temperatures at which the phases are at least metastable. The free energies of both phases were determined from 1200 K to 2000 K at zero pressure. All simulations employed 1 fs timesteps.

Determining the non-equilibrium free energies of the phases required three steps. First we found the spring constants for harmonic approximations to the β- and α-phases within an NPT ensemble with a Nosé-Hoover barostat and Langevin thermostat at zero pressure and 1200 K, averaged over 10 ps. For an equiaxed cell with ∼40,000 atoms we found the spring constants to be 1.36 eV/Å^2 for β and 2.17 eV/Å^2 for α.

The second step is integration along the Frenkel-Ladd path[18] to find the free energy of each phase at the lower limit of the temperature range of interest, for which we used a NVT ensemble with a Langevin thermostat set to 1200 K. The switching procedure took 20 ps and equilibrated for 4 ps. From this, the free energies at 1200 K for β- and α-phases were determined to be -5.368 eV/atom and -5.379 eV/atom, indicating that α is stable at this temperature.

Using these values as reference points, the remainder of the non-equilibrium free energy curves were determined using reversible scaling[19,20] of the MEAM potential in the third step. Reversible scaling was done with a NPT ensemble with a Nose-Hoover barostat and a Langevin thermostat from 1200 K to 2000 K. The forward and backward simulations were 100 ps. To ensure that a sufficiently large supercell was used, the transition temperature was calculated for multiple supercell sizes. β supercells with side lengths which were multiples of 3 conventional bcc unit cells in the range $9 \times 9 \times 9$ (1458 atoms) to $30 \times 30 \times 30$ (54000 atoms) were used. For each size, a corresponding α supercell was chosen to be approximately equiaxed and have a similar number of atoms to the β supercells. The free energy curves calculated for the largest supercells are shown in Figure 1a, and yield a transition temperature of 1694 K. The β to α transition temperature was found to vary with supercell size, as shown in Figure 1, but our largest simulations indicate a value of ∼1700 K.

This value differs significantly from that given by Hennig *et al.* (1250 K), the creators of this MEAM potential[16]. To verify the accuracy of our reversible scaling method calculation, we also performed a series of coexistence calculations, where the interface between the two

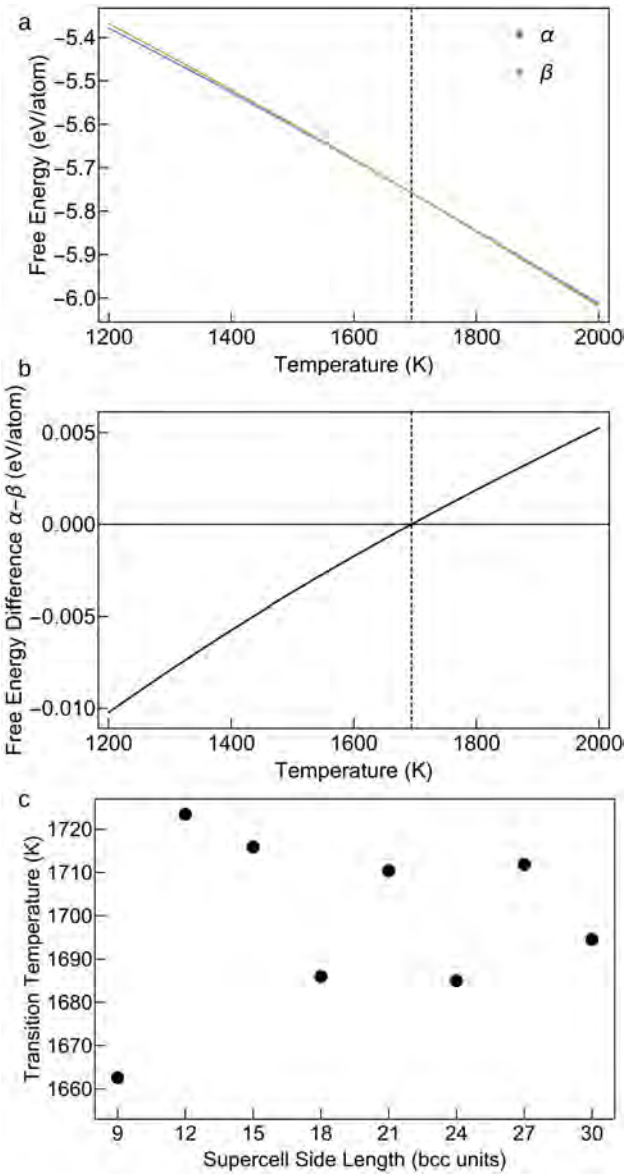

FIG. 1. (a) Free energies of the hcp and bcc phases calculated using the reversible scaling method with the $30 \times 30 \times 30$ bcc unit supercell size. (b) Free energy difference corresponding to (a). (c) Variation of the transition temperature with supercell size.

phases was designed to be coherent and to reflect the elastic constants of both phases at high temperature, such that it would minimally influence phase evolution. In these calculations we begin with a supercell containing half α and half β titanium, meeting at an interface that satisfies the Burgers orientation relation. The elastic energy of the combined system can be expressed as

$$E = \frac{V_\alpha}{2} C^\alpha_{ijkl} \eta^\alpha_{ij} \eta^\alpha_{kl} + \frac{V_\beta}{2} C^\beta_{ijkl} \eta^\beta_{ij} \eta^\beta_{kl}, \tag{1}$$

where V_α (V_β) refers to the volume of the α (β) phase, $\boldsymbol{C}^\alpha$ ($\boldsymbol{C}^\beta$) corresponds to the elastic constants of the respective phases in the given frame of reference, and $\boldsymbol{\eta}_\alpha$ ($\boldsymbol{\eta}_\beta$) refers to the strain applied to the given phase. By applying the constraint that the lattice vectors parallel to the interface must match for both phases, the supercell can be constructed by solving for the strains $\boldsymbol{\eta}^\alpha$ and $\boldsymbol{\eta}^\beta$. This can be expressed as a system of equations of the following form:

$$a_0^\alpha(1+\eta_{11}^\alpha) = a_0^\beta(1+\eta_{11}^\beta), \tag{2a}$$

$$a_0^\alpha(1+\eta_{22}^\alpha) = \sqrt{2}a_0^\beta(1+\eta_{22}^\beta), \tag{2b}$$

$$\frac{\partial E}{\partial \eta_{33}^\alpha} = 0, \tag{2c}$$

$$\frac{\partial E}{\partial \eta_{33}^\beta} = 0, \tag{2d}$$

$$\frac{\partial E}{\partial \eta_{11}^\alpha} = 0, \tag{2e}$$

$$\frac{\partial E}{\partial \eta_{22}^\alpha} = 0, \tag{2f}$$

with a_0^α and a_0^β being the equilibrium lattice parameters of the α and β phases.

NPT-ensemble molecular dynamics simulations at temperatures ranging from 1200 K to 1800 K were performed using these coexistence supercells containing 17600 atoms. At temperatures 1700 K and below, the supercell transformed entirely to α. At temperatures 1712.5 K and above, the supercell transformed entirely to β. This indicates a transition temperature slightly above 1700 K, which is in excellent agreement our reversible scaling calculations. This also agrees well with the value 1720 K recently calculated by Dickel *et al.* for this MEAM potential[21].

The large difference between the temperature at which α becomes the more stable phase (1700 K) and the temperature at which β rapidly transforms to α homogeneously in very small (432 atom) supercells (1250 K) highlights the usefulness of non-equilibrium thermodynamic integration for potential validation. The following sections detail simulations of the β to α transition, which were performed at temperatures in the range 1050 K to 1400 K, well below the transition temperature for this potential. Unfortunately the large difference between the β to α transition temperature in this MEAM potential and that of actual titanium (1155 K[22]) means the behavior at a given temperature in our simulations cannot be directly compared to that in experiment at the same temperature. Nevertheless, we expect

that the qualitative properties of the transition will be well represented by the potential.

B. Dislocation Supercell Construction

For all dislocation calculations we use periodic screw dislocation arrays arranged such that each dislocation has four nearest neighbor dislocations, and is opposite in Burgers vector direction to its nearest neighbors. These arrangements are known as quadrupolar, and minimize the elastic energy of a periodic dislocation array due to cancellation of long-range stress fields[23]. The line direction of all dislocations is $[1\ 1\ 1]_\beta$, and therefore the Burgers vectors for the screw dislocations are $\pm\frac{a_0}{2}[1\ 1\ 1]_\beta$. Dislocation-containing supercells are oriented such that $[1\ 1\ \bar{2}]_\beta$ is parallel to the x-axis, the line direction/Burgers vector $[1\ 1\ 1]_\beta$ is parallel to the y-axis, and $[\bar{1}\ 1\ 0]_\beta$ is parallel to the z-axis. Supercell lattice vectors are tilted to account for the distortion from the dislocations as prescribed by Lehto and Öberg[24]. Initial displacements were determined using the method of Daw[23], which yields good starting points that account for elastic anisotropy while only requiring lattice parameters and elastic constants as inputs.

The quadrupolar arrangement used in this paper had dislocations of alternating sign on the $(\bar{1}\ 1\ 0)_\beta$ and $(1\ 1\ \bar{2})_\beta$ planes (i.e. along the x and z directions). The superlattice vectors in these directions were 244 Å and 141 Å. For the majority of the calculations presented the superlattice vector along the dislocation line direction was 46 Å and the supercell contained 86,400 atoms.

Stabilization of the dislocations within the supercell proved to be challenging. The positions produced from our linear elasticity method resulted in nearly immediate annihilation of the dislocations at any simulated temperature. Relaxation of the positions at 0 K can often solve this type of issue, but the bcc structure is not stable in pure Ti at 0 K. To get around these issues, we scaled the lattice vectors and atomic coordinates to those of tungsten, and relaxed the supercell to a force tolerance of 10^{-4} eV/Å within a tungsten Finnis-Sinclair EAM potential[25] for which bcc is the stable phase from 0 K to at least 1350 K. With the relaxed cell and still within the tungsten potential, an NPT ensemble with a Nose-Hoover barostat and Langevin thermostat set at 0 pressure and 1350 K was used to achieve an equilibrated state over 100 ps. This equilibrated configuration was then scaled to the lattice parameters of titanium (estimated via molecular dynamics without dislocations)

and the atoms converted to Ti.

Structural analysis of the dislocation cells before and after transformation was performed using the OVITO software package[26]. Chiefly the polyhedral template matching (PTM)[27] tool was used to identify the local structure as well as orientation at each atomic site. Averaging of the atomic coordinates over 100 fs was performed within LAMMPS to smooth thermal vibrations and allow for PTM calculation.

C. Calculation of Elastic Constants

The elastic constants at finite temperature were calculated by first allowing the supercell to equilibrate at temperature in an NPT ensemble for 100 ps. NVT ensembles were then simulated for 100 ps for 24 separate deformations corresponding to the six unique strain components (ε_{11}, ε_{22}, ε_{33}, ε_{23}, ε_{13}, ε_{12}) at four different magnitudes of strain each (ranging from strains of -0.01 to 0.01). By fitting the line between the stress calculated from the sum of the kinetic energy tensor and virial tensor[28] with each strain component, all 21 unique elastic constants could be determined. For more information on the calculation, see reference[29].

The uncertainty associated with the above calculation was approximated by first determining the correlation time of each stress component for every applied strain. This was used to estimate the error in stress using the bootstrap method[30]. The error in the elastic constants was then estimated by performing 100 linear fits between stress and strain components corresponding to each elastic constant, where for each fit the stresses were randomly generated to be within the error range calculated for the specific stress component. The elastic constant was then considered to be the mean of these fittings with the error being the standard error of the mean.

The elastic constants of β-Ti were calculated for temperatures ranging from 1200 K to 1700 K. At all temperatures considered the β phase was shown to be elastically stable. However, C_{12} gradually approaches C_{11} with decreasing temperature, meaning that the shear modulus ($C' = \frac{1}{2}(C_{11} - C_{12})$) steadily softens. This is associated with a consistent increase in the Zener anisotropy ($A_Z = \frac{2C_{44}}{C_{11}-C_{12}}$) as shown in Table I and results in a softening of the N-point phonon associated with the Burgers transformation[1]. Ogi *et al.* found experimentally that the elastic constants of β-Ti vary weakly with temperature[31], which agrees well with

our calculated elastic constants.

TABLE I. Calculated elastic constants of β-Ti at finite temperatures within the MEAM potential, and elastic constants measured in previous experimental studies.

Temperature	C_{11} (GPa)	C_{12} (GPa)	C_{44} (GPa)	C' (GPa)	A_Z
1200 K	89.1 ± 0.6	81.0 ± 0.3	37.0 ± 0.7	4.1 ± 0.5	9.2 ± 0.8
1300 K	89.4 ± 0.7	79.9 ± 0.2	37.2 ± 0.3	4.7 ± 0.5	7.8 ± 0.6
1400 K	89.3 ± 0.5	78.5 ± 1.0	36.8 ± 0.1	5.4 ± 0.8	6.8 ± 0.7
1500 K	88.9 ± 1.1	77.4 ± 0.2	36.4 ± 0.4	5.6 ± 0.7	6.4 ± 0.6
1600 K	88.7 ± 0.7	76.7 ± 0.7	35.8 ± 0.1	6.0 ± 0.7	5.9 ± 0.5
1700 K	88.1 ± 0.8	75.6 ± 0.3	35.1 ± 0.4	6.3 ± 0.6	5.6 ± 0.4
1293 K[22]	134	110	36	12	3
1273 K[32]	99	85	33.6	7	4.8
1273 K[33]	97.7	82.7	37.5	7.5	5

III. RESULTS

A. Elasticity Theory Analysis

The prediction of variant selection from elasticity theory is not a new idea. Cahn used isotropic elasticity theory to analyze the nucleation of second phases on dislocations[34], while Thomas and Nutting proposed that the preferred variants to nucleate from a dislocation are those that best accommodate the strain field of a dislocation[35]. More recently, Qiu *et al.* considered the variant selection of α precipitates nucleating from both edge and screw dislocations in β-Ti using both anisotropic elasticity theory and phase field modeling[12]. They found that during nucleation the preferred variants are those with the most negative elastic interaction energy associated with the strain field of the dislocation. However, they saw that the most dominant variants in growth were those for which the habit plane was oriented nearly parallel with the dislocation line, an idea first proposed by Kelly and Nicholson[36].

Here, only the preferential nucleation of variants on the dislocation are considered. These variants will have the geometry imposed by our few-layer supercells, and therefore make for a good point of comparison. This geometry also represents the observations in the early stages

of nucleation in our many-layer supercells. As a result, an approach similar to Thomas and Nutting's proposed mechanism of variant selection is used in an anisotropic elasticity model to identify the variants most likely to nucleate from a screw dislocation in β-Ti, with the strain field of the straight $\langle 1\ 1\ 1\rangle_\beta$-type dislocation generated from continuum anisotropic linear elasticity theory[37].

1. *Burgers Transformation Path*

To understand the nucleation of the α phase from the β phase at the screw dislocation core, a comparison has been made of the strain field produced by such a dislocation with the strain state necessary for the Burgers transformation[1]. The Burgers path consists of both a strain and shuffling of atoms. The shuffling of atomic $\{1\ 1\ 0\}_\beta$ planes is associated with the N-point phonon while the transformation strain can be represented as eigenstrains for the orientations $\boldsymbol{a} = \langle 1\ 1\ 0\rangle_\beta$, $\boldsymbol{b} = \langle 0\ 0\ 1\rangle_\beta$, and $\boldsymbol{c} = \langle 1\ \bar{1}\ 0\rangle_\beta$. The eigenstrains consist of a compressive strain along $\langle 0\ 0\ 1\rangle_\beta$ and a tensile strain along $\langle 1\ 1\ 0\rangle_\beta$. The Burgers transformation results in the α/β orientation relation $\{1\ 1\ 0\}_\beta||(0\ 0\ 0\ 1)_\alpha$ (see Table II for all variants).

The lattice parameter of β-Ti was found to be $a_\beta = 3.32$ Å at 1200 K, while the lattice parameters for the α phase were estimated to be $a_\alpha = 2.97$ Å and $c_\alpha = 4.77$ Å. The Lagrangian strain is written in Einstein summation notation as

$$\varepsilon_{jk} = \frac{1}{2}\left(F_{mj}F_{mk} - \delta_{jk}\right). \tag{3}$$

Here $\boldsymbol{F}$ is the deformation gradient, defined as $F_{mj} = \frac{\partial x_m}{\partial X_j}$ ($\boldsymbol{x}$ corresponds to the current configuration and $\boldsymbol{X}$ the reference configuration), and δ_{jk} is the Kronecker Delta. Setting the lattice vectors of the reference frame to be those defined above, the transformation strain is

$$\boldsymbol{\varepsilon}^0 = \begin{pmatrix} 0.101 & 0 & 0 \\ 0 & -0.099 & 0 \\ 0 & 0 & 0.016 \end{pmatrix}. \tag{4}$$

2. *Dislocation Induced Nucleation*

To predict the variants that will nucleate on the dislocation and the orientations along which they will grow, a comparison was made between the strain associated with the Burgers transformation path and the stress field resulting from a single $\langle 1\ 1\ 1\rangle_\beta$-type dislocation a distance r_{core} away from the center of the dislocation, with r_{core} being an estimate for the dislocation core radius using elasticity theory[38]. This was done by calculating the elastic energy density, taking into consideration the orientation of the α nucleus to the dislocation as well as the orientation relationship between the β and α phases. As shown in Table II, there exist 12 unique variants associated with the Burgers transformation between the β and α phases[1,39]. With respect to the nucleation of a general α precipitate, there are six unique habit planes in the β phase for which there are two unique variants. These two variants are related by a $\frac{\pi}{2}$ rotation perpendicular to the habit plane. The elastic interaction between an Eshelby inclusion with strain equal to the Burgers transformation strain for variant n (Equation 4) and the stress induced by a $[1\ 1\ 1]_\beta$-type screw dislocation as a function of angle θ around the dislocation ($\theta = 0$ corresponds to the direction $[1\ 1\ \bar{2}]_\beta$ and $\theta = \frac{\pi}{2}$ to the direction $[1\ \bar{1}\ 0]_\beta$) can be assessed by computing the energy density $e_n^{int}(\theta)$, following Qiu *et al.*[12]:

$$e_n^{int}(\theta) = -\sigma_{ij}(\theta)\epsilon_{ij}^0(V_n) \tag{5}$$

here $\sigma(\theta)$ is the stress induced by the screw dislocation at radius $r_{core} = 5.90$ Å from the dislocation origin and $\epsilon_{ij}^0(V_n)$ is the Burgers transformation strain associated with the n^{th} variant.

Plotting all twelve unique variants (Figure 2) it is apparent that there is an absolute minimum value that is obtained by three variants. The orientations at which a variant displays an absolute minimum are: variant 4 near $\frac{\pi}{2}$, variant 8 near $\frac{7\pi}{6}$, and variant 12 near $\frac{11\pi}{6}$. These are also the three variants that satisfy the additional constraint proposed by Kelly and Nicholson[36] that the Burgers vector in the β phase is contained by the α habit plane (i.e. $[1\ 1\ 1]_\beta \parallel [1\ 1\ \bar{2}\ 0]_\alpha$). These three variant and orientation pairs are the same as those along which α precipitates are shown to nucleate in MD simulations. If the sign of the dislocation Burgers vector is reversed in the calculation the same three variants are found to be favored, but with minima rotated by π, also in agreement with our MD simulations. All inputs used for the dislocation strain field calculation ($a_\beta, C_{11}, C_{12}, C_{44}$) were calculated

TABLE II. List of the 12 unique variants for the Burgers orientation between the α and β precipitates[1,39].

Variant	Plane Relation	Direction Relations	
V1	$(1\ 1\ 0)_\beta \parallel (0\ 0\ 0\ 1)_\alpha$	$[\bar{1}\ 1\ \bar{1}]_\beta \parallel [1\ 1\ \bar{2}\ 0]_\alpha$	$[\bar{1}\ 1\ 2]_\beta \parallel [\bar{1}\ 1\ 0\ 0]_\alpha$
V2	$(1\ 1\ 0)_\beta \parallel (0\ 0\ 0\ 1)_\alpha$	$[\bar{1}\ 1\ 1]_\beta \parallel [1\ 1\ \bar{2}\ 0]_\alpha$	$[\bar{1}\ 1\ \bar{2}]_\beta \parallel [\bar{1}\ 1\ 0\ 0]_\alpha$
V3	$(\bar{1}\ 1\ 0)_\beta \parallel (0\ 0\ 0\ 1)_\alpha$	$[1\ 1\ \bar{1}]_\beta \parallel [1\ 1\ \bar{2}\ 0]_\alpha$	$[1\ 1\ 2]_\beta \parallel [\bar{1}\ 1\ 0\ 0]_\alpha$
V4	$(\bar{1}\ 1\ 0)_\beta \parallel (0\ 0\ 0\ 1)_\alpha$	$[1\ 1\ 1]_\beta \parallel [1\ 1\ \bar{2}\ 0]_\alpha$	$[1\ 1\ \bar{2}]_\beta \parallel [\bar{1}\ 1\ 0\ 0]_\alpha$
V5	$(0\ 1\ 1)_\beta \parallel (0\ 0\ 0\ 1)_\alpha$	$[\bar{1}\ \bar{1}\ 1]_\beta \parallel [1\ 1\ \bar{2}\ 0]_\alpha$	$[\bar{2}\ 1\ \bar{1}]_\beta \parallel [\bar{1}\ 1\ 0\ 0]_\alpha$
V6	$(0\ 1\ 1)_\beta \parallel (0\ 0\ 0\ 1)_\alpha$	$[1\ \bar{1}\ 1]_\beta \parallel [1\ 1\ \bar{2}\ 0]_\alpha$	$[2\ 1\ \bar{1}]_\beta \parallel [\bar{1}\ 1\ 0\ 0]_\alpha$
V7	$(0\ \bar{1}\ 1)_\beta \parallel (0\ 0\ 0\ 1)_\alpha$	$[\bar{1}\ 1\ 1]_\beta \parallel [1\ 1\ \bar{2}\ 0]_\alpha$	$[2\ 1\ 1]_\beta \parallel [\bar{1}\ 1\ 0\ 0]_\alpha$
V8	$(0\ \bar{1}\ 1)_\beta \parallel (0\ 0\ 0\ 1)_\alpha$	$[1\ 1\ 1]_\beta \parallel [1\ 1\ \bar{2}\ 0]_\alpha$	$[\bar{2}\ 1\ 1]_\beta \parallel [\bar{1}\ 1\ 0\ 0]_\alpha$
V9	$(1\ 0\ 1)_\beta \parallel (0\ 0\ 0\ 1)_\alpha$	$[\bar{1}\ 1\ 1]_\beta \parallel [1\ 1\ \bar{2}\ 0]_\alpha$	$[1\ 2\ \bar{1}]_\beta \parallel [\bar{1}\ 1\ 0\ 0]_\alpha$
V10	$(1\ 0\ 1)_\beta \parallel (0\ 0\ 0\ 1)_\alpha$	$[\bar{1}\ \bar{1}\ 1]_\beta \parallel [1\ 1\ \bar{2}\ 0]_\alpha$	$[1\ \bar{2}\ \bar{1}]_\beta \parallel [\bar{1}\ 1\ 0\ 0]_\alpha$
V11	$(\bar{1}\ 0\ 1)_\beta \parallel (0\ 0\ 0\ 1)_\alpha$	$[1\ \bar{1}\ 1]_\beta \parallel [1\ 1\ \bar{2}\ 0]_\alpha$	$[1\ 2\ 1]_\beta \parallel [\bar{1}\ 1\ 0\ 0]_\alpha$
V12	$(\bar{1}\ 0\ 1)_\beta \parallel (0\ 0\ 0\ 1)_\alpha$	$[1\ 1\ 1]_\beta \parallel [1\ 1\ \bar{2}\ 0]_\alpha$	$[1\ \bar{2}\ 1]_\beta \parallel [\bar{1}\ 1\ 0\ 0]_\alpha$

for β-Ti at 1200 K. See the Section II for further details. Similar behavior is predicted over a wide range of elastic constant values, which indicates that this variant selection is not peculiar to the MEAM potential chosen.

B. Few-Layer Supercell Molecular Dynamics

We begin with a β supercell with 16 layers along the dislocation line (86,400 atoms). Molecular dynamics simulations starting with both a reference undeformed supercell and a stabilized titanium supercell containing two dislocations were performed with an NPT ensemble using a Nosé-Hoover barostat and Langevin thermostat at zero pressure and temperatures of 1050 K, 1200 K, 1225 K, 1250 K, 1275 K, 1300 K, 1350 K, and 1400 K. For each cell at each temperature ten independently-seeded simulations 500 ps in length were performed, for a total of 160 simulations in this group.

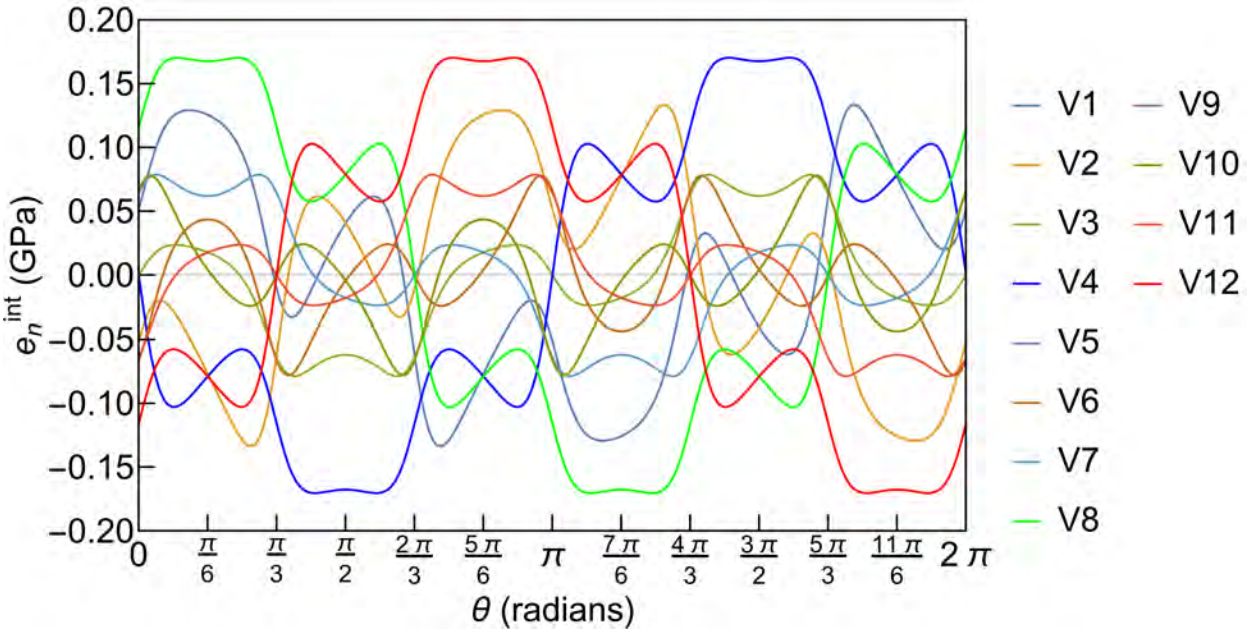

FIG. 2. Plot of interaction energy density $e_n^{int}(\theta)$ with respect to direction symbolized by the angle θ. The absolute minima occur at $\frac{\pi}{2}$, $\frac{7\pi}{6}$, and $\frac{11\pi}{6}$ in agreement with molecular dynamics simulations. $\theta = 0$ corresponds to the direction $[1\ 1\ \bar{2}]_\beta$ and $\theta = \frac{\pi}{2}$ to the direction $[1\ \bar{1}\ 0]_\beta$.

A typical simulation result is shown in Figure 3. The visualization presented is from OVITO. PTM was used first to identify a local crystal structure at each atom, using a root-mean-squared deviation (RMSD) cutoff of 0.09 (i.e. atoms above this threshhold are identified as "other" and colored white). The atoms found to be bcc are then colored black. For the atoms identified as hcp, the coloring is by the y-component of the orientation identified by PTM. This is very useful for distinguishing the α variants. An undocumented bonus-feature of PTM exists for the hcp crystal structure. Because there are two basis atoms in hcp, two slightly different orientations are identified within the same grain, alternating on adjacent basal planes. This leads to a striped appearance in our visualizations that allows us to easily identify basal planes. In this color scheme variant 4 appears blue, variant 8 is yellow-green, and variant 12 is red.

Examining all trials, we see three dominant variants (V4, V8, and V12) of α grains, in agreement with our elasticity theory prediction. The angles at which these variants appear are also in agreement with our prediction. Examples of all orientations are shown in Figure 4. It is worth noting that because the two dislocations have oppositely signed Burgers vectors, the direction in which each variant nucleates is rotated by π when considering the right-

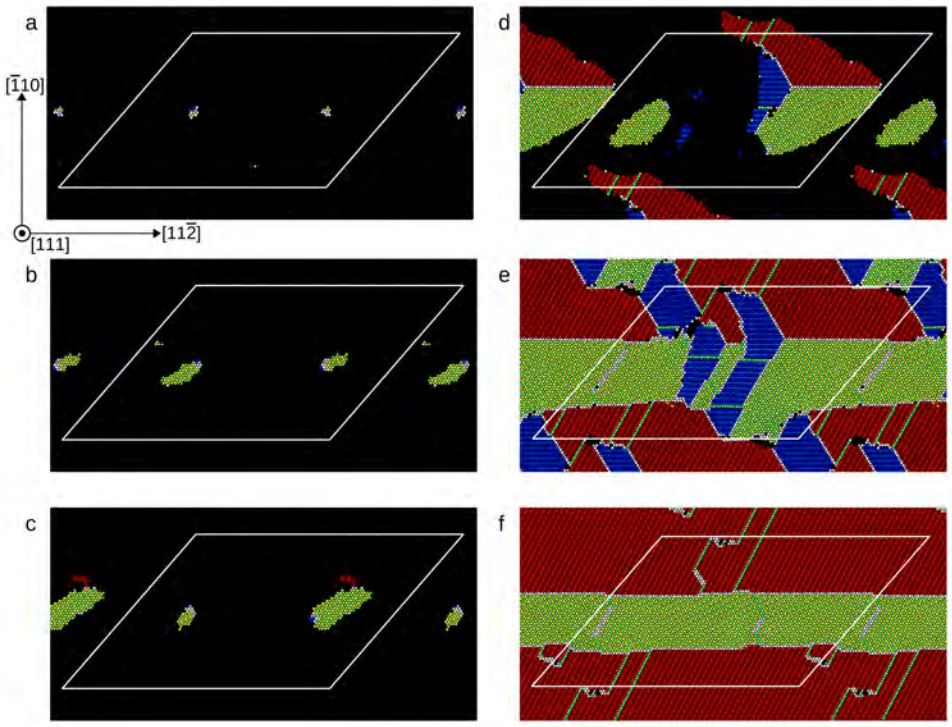

FIG. 3. Nucleation and growth of the α phase (colored atoms) from the β phase (black) at 1225 K viewed in the plane perpendicular to the dislocation line direction. Coloring is by PTM as described above. White atoms have no identified structure in PTM within the RMSD cutoff of 0.09, and correspond to dislocations, grain boundaries, or point defects. (a) 0 ps: initial dislocation cell, (b) 20 ps: initial nucleation of α phase at each dislocation, (c) 40 ps: growth of primary nuclei and formation of a secondary nucleus adjacent to the right-hand nucleus, (d) 60 ps: continued growth and formation of secondary nucleus complementary to the primary and previous secondary nuclei, (e) 80 ps: completed growth of fine-grained α, (f) 500 ps: coarsening has occured and removed all high-energy grain boundaries.

hand dislocation (Burgers vector into page) vs. the left-hand dislocation (Burgers vector out of page). Due to concerns about the validity of the MEAM potential employed stemming from its incorrect transition temperature, a limited set of calculations of this same type were also performed using the MEAM potential due to Dickel *et al.*[40]. Exactly the same variant selection behavior was found within this more recent potential, in agreement with the predictions presented here.

Using PTM through OVITO, we can extract both phase and orientation information

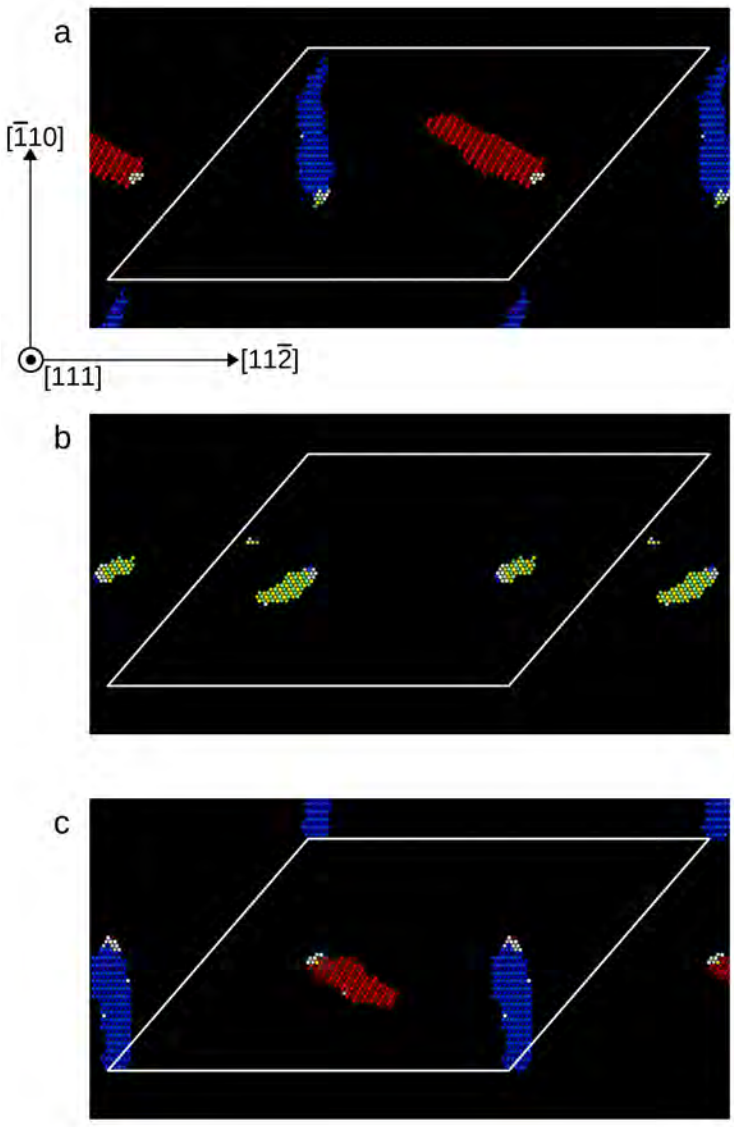

FIG. 4. Examples of all three dominant orientations nucleating on both the left-hand and right-hand dislocations. Coloring is by PTM as described above.

over time rapidly from all our simulations. Figure 5 shows the fraction of atoms identified as belonging to each variant type for the same simulation as shown in Figure 3. At approximately 50 ps the primary V8 nuclei form, followed quickly by secondary nuclei of the other two dominant variants. Transformation to α is complete at 100 ps. Following this, growth of V12 grains at the expense of V4 leads to the coarse structure seen in Figure 3f.

Taking the total fraction of hcp atoms we fit the growth to the following Avrami-type

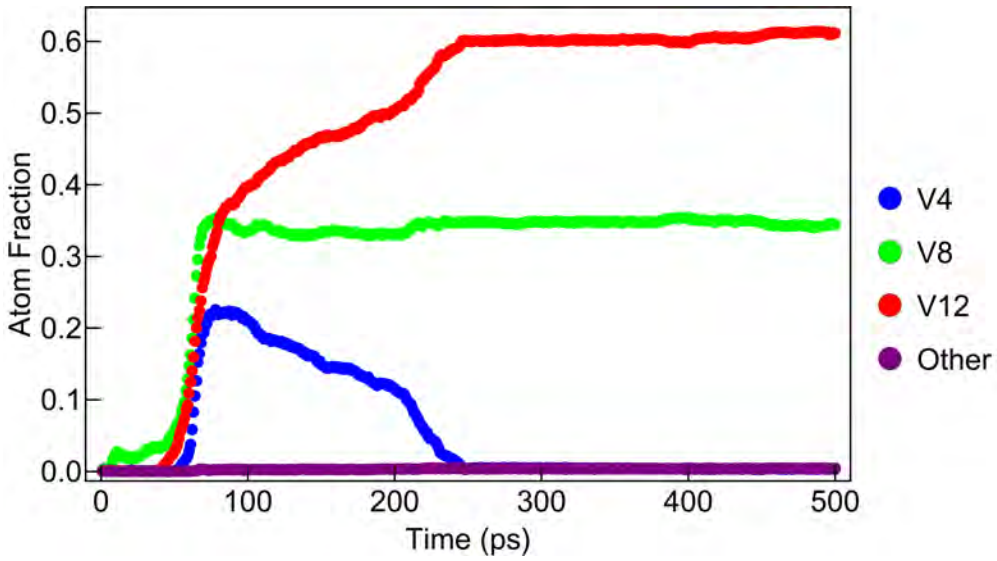

FIG. 5. Atom fraction of α V4, V8, V12, and other (i.e. hcp atoms not matching any of the three dominant variants) for the simulation at 1225 K shown in Figure 3.

equation[41–43]:

$$\begin{cases} 0 & t < t_{het} \\ \alpha_{max}(1 - \exp -(\frac{t-t_{het}}{\tau})^3) + N_0 & t \geq t_{het} \end{cases} \tag{6}$$

to find the characteristic growth time (τ). This fit is shown for our example simulation in Figure 6. In our fit, we allow also fit the nucleation time before rapid growth begins, which yields a good estimate of the time to heterogeneous nucleation (t_{het}). α_{max} is the (known) maximum fraction of the supercell which is transformed to α (0.5% to 5% of the supercell is identified as having no phase or remaining β after transformation). N_0 is a small offset allowed in the fit, and was less than 10^{-5} in all samples.

In our simulations starting from the configuration containing dislocations we observe a transformation to α in all trials at temperatures 1250 K and below. At 1275 K we observed two trials transform, while the other eight remained in the β phase. At temperatures 1300 K and above all trials remained in the β phase. The results of our fits for all simulations at 1050 K, 1200 K, 1225 K, and 1250 K are summarized in Table III. When simulations were started from the configuration without dislocations, transformation was only observed at 1050 K, demonstrating the necessity of heterogeneous nucleation sites to induce transformation.

From the simulations of the supercell without dislocations we measure t_{hom}, the homogeneous equivalent to t_{het}. At 1050 K, t_{hom} was 91.8 ± 51.0 ps, which is both much longer and

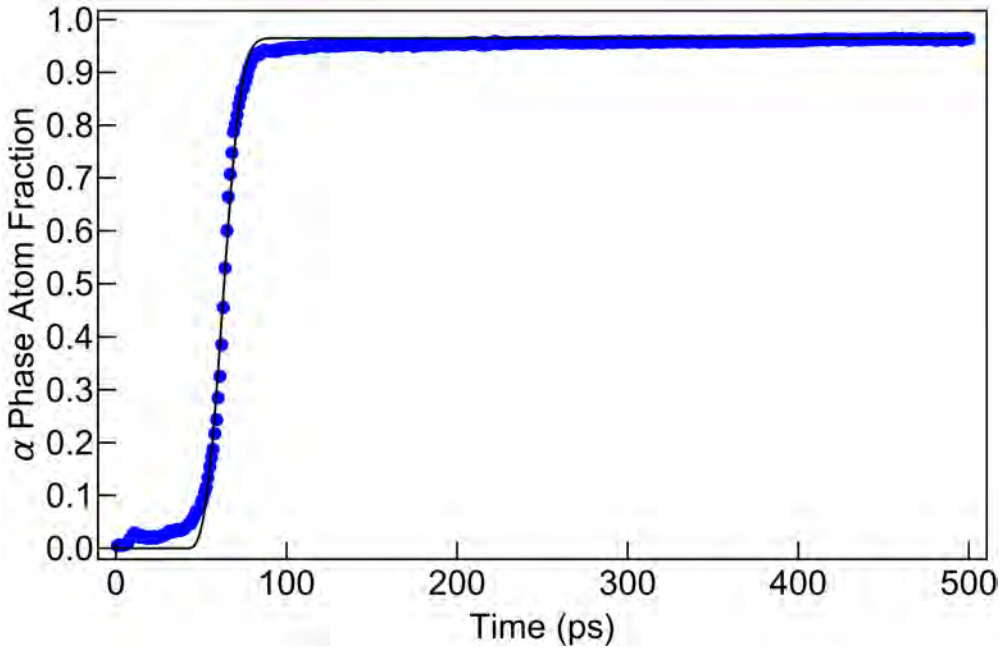

FIG. 6. Avrami equation fit (black line) to α phase nucleation and growth data (blue points) for the simulation at 1225 K shown in Figure 3.

TABLE III. Heterogeneous nucleation time t_{het} and transformation characteristic time τ from Avrami equation fits to data from simulations containing dislocations.

Temperature	1050 K	1200 K	1225 K	1250 K
t_{het} (ps)	1.95 ± 0.86	18.5 ± 3.7	36.4 ± 14.0	104.3 ± 30.0
τ (ps)	8.3 ± 1.0	16.2 ± 1.8	20.3 ± 2.3	22.5 ± 1.6

much more varied than the heterogeneous case at the same temperature. This demonstrates the potency of the dislocation lines as heterogeneous nucleation sites. In fact, the nucleation behavior without dislocations at 1050 K is similar to that with dislocations at 1250 K. In terms of growth rate, τ at 1050 K without dislocations was 9.1 ± 1.2 ps, which is similar to but a bit slower than the rate with dislocations. This indicates that the strain from the dislocation may provide a boost to the α phase growth rate.

C. Many-Layer Supercell Molecular Dynamics

Following the procedure detailed in Section II for stabilizing dislocations in high temperature β-Ti, we created a new supercell with 256 layers along the dislocation line direction

and the same area on the face normal to this direction as used previously, with a total of 1,382,400 atoms. This supercell is much longer along the line direction (737 Å) than the separation between the dislocations (183 Å). Nucleation of the α phase in this supercell was observed in two molecular dynamics simulations at 1250 K with NPT ensemble configured as described previously. Early in this process it is apparent that various small proto-nuclei form, fail to reach critical radius, and disappear. These nucleate with the same orientations as observed in the shorter supercells, but do not span the entire length of the simulation cell. It is also noteworthy that while all three possible orientations are sometimes present on the same dislocation line, they were not observed at the same point along the line at the same time. This is likely due to the elastic field around a nucleus making formation of a nearby nucleus of differing orientation on the dislocation line less favorable.

While we were not able to conduct enough simulations to facilitate a detailed statistical analysis, it is clear that the nucleation rate (of supercritical nuclei) in the long supercells is lower than in the short supercell at the same temperature. Fitting to the Avrami equation yields nucleation times of 134 ps and 139 ps for the two samples, which are both approximately one standard deviation longer than for the few-layer supercell at the same temperature. The characteristic growth times were 37.9 ps and 30.8 ps, which indicates much slower growth than in the short supercells. In the short supercell once a proto-nucleus is formed it need not grow very far before it runs into its own image through a periodic boundary and at this point its length becomes effectively infinite. When the superlattice vector along the line direction is larger than the critical nucleus size, the nuclei exist for much longer before this occurs. During this stage the surface energy due to the nucleus surfaces normal to the dislocation line direction increase the energy of the nucleus. Furthermore, as a nucleus grows along the dislocation line it must compete with nuclei of other orientations that it encounters, as it is unfavorable for two nuclei of differing orientations to exist in the same region of the dislocation line at the same time. This progression can be observed in Figure 7.[44]

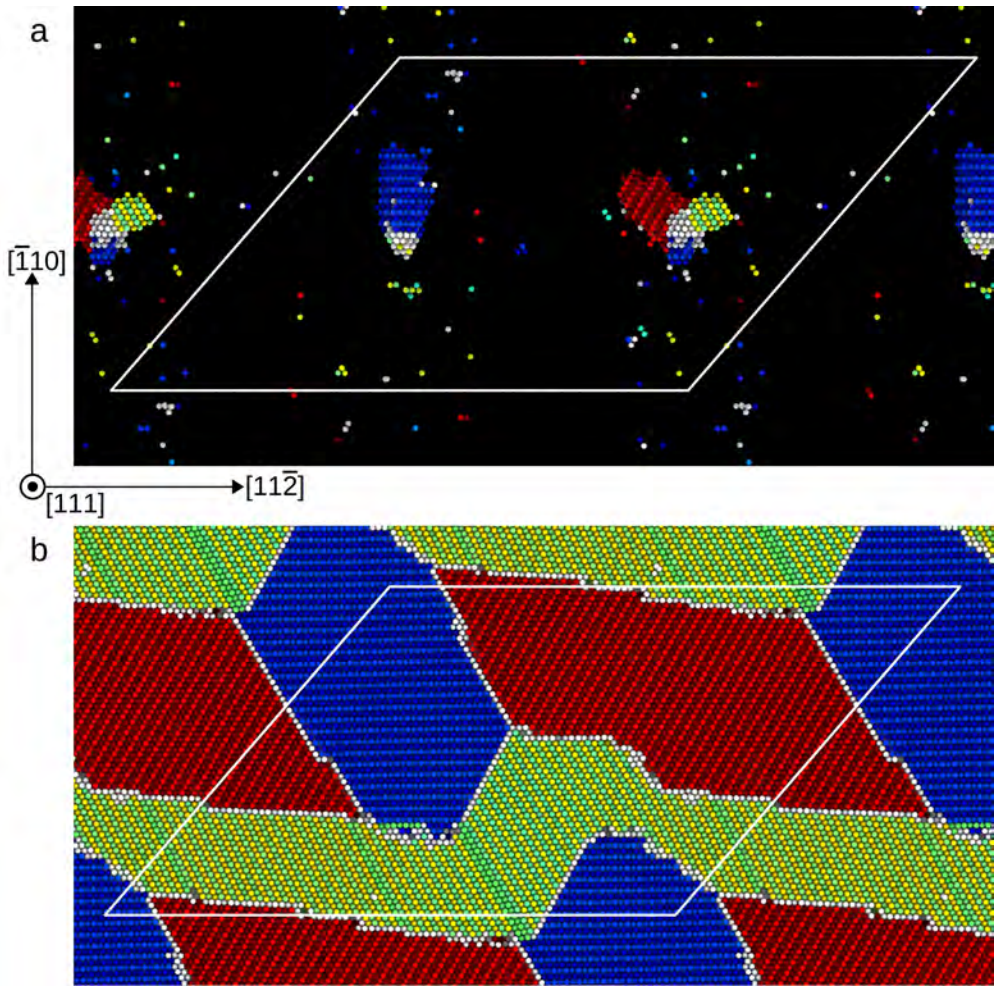

FIG. 7. Front view of nucleation and growth of the α-phase from β (atoms removed) at 1250 K along the $[111]_\beta$ screw dislocation lines in the supercell which is 737 Å in length. Atom coloring is by PTM as described previously. (a) Configuration 40 ps into simulation, shows single nucleus on left-hand dislocation and a number of smaller nuclei on the right-hand dislocation. These occupy different segments of the line in the direction into the page. (b) Post-transformation microstructure 210 ps into simulation. The somewhat columnar structure is similar to that found in the few-layer supercells, though not all grains completely fill the length of the supercell.

IV. DISCUSSION

A. Nucleation Times and Transformation Rates

The increase in time to a successful α nucleation event with increasing temperature is significant. Over the range 1200 K to 1250 K the increase is 5×. On the other hand, the

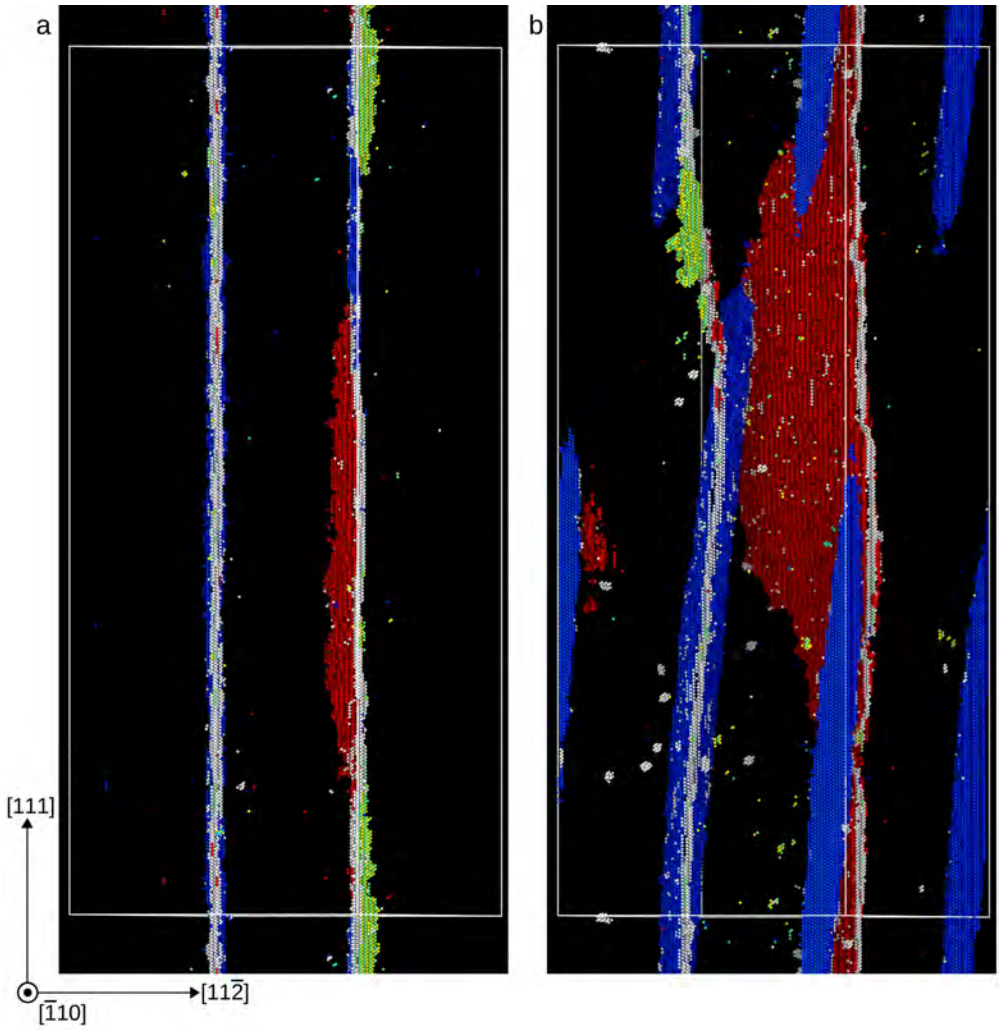

FIG. 8. Bottom view of nucleation and growth of the α-phase from β (atoms removed) at 1250 K along the $[111]_\beta$ screw dislocation lines in the supercell which is 737 Å in length. Atom coloring is by PTM as described previously. (a) Configuration 40 ps into simulation, shows single nucleus on left-hand dislocation and a number of smaller nuclei on the right-hand dislocation. (b) 150 ps into simulation. This view most clearly shows the change of habit plane by the left-hand nucleus, and how this leads to detachment of part of the nucleus from the dislocation line.

change in this time with respect to supercell length is small. In the many-layer supercells, the time to form a supercritical nucleus is slightly longer than in the few-layer supercells. Probably this is due to competition between two factors: (1) there is 16× more dislocation line length on which to form a nucleus, which ought to increase the rate and (2) the size of a supercritical nucleus is larger, because the nuclei do not immediately cross the periodic

boundaries and contact themselves.

In the few-layer supercells, growth rates drop consistently as temperature increases due to the lower driving force to form α. The growth rate in the many-layer supercell is much slower. This results from competition between neighboring nuclei with different orientations on the same dislocation line, as well as the increase in surface area of the nuclei due to their curved edges before they completely fill the supercell. It also appears that there is little growth of the nuclei while they change in habit plane and pull away from parts of the dislocation. In fact, there is some local shrinkage of supercritical nuclei where they pull away from the dislocation line.

The success of Equation 6 in fitting the nucleation and growth data (as shown in Figure 6) is mildly surprising, as the model was derived to represent homogeneous nucleation and growth at a constant rate. In our simulations (other than that without dislocations at 1050 K) the observed nucleation is plainly heterogeneous on the dislocation lines. However, nucleation does not end there. Strain-induced nucleation of secondary grains adjacent to the primary grains allows the growth to continue at a greater rate than if only primary nucleation on the dislocation lines occurred. However, this is still not truly homogeneous nucleation because it is induced only within a range (approximately 30 Å) of existing nuclei. On the other hand, these secondary nuclei induce more secondary nuclei to form, and thus can spread the α phase rapidly. Therefore while primary nucleation is heterogeneous on dislocation lines only, secondary nucleation events occur throughout the supercell.

B. Habit Plane Analysis

In the few-layer geometry the length of the supercell along the dislocation line direction is as short as possible (without altering the transition temperature significantly, see Figure 1) so that the separation between the dislocations can be maximized within resource limitations. This effectively fixes the line direction of the dislocations, which is generally acceptable because the line direction has been chosen to be one known to be common in the material. In the case of phase nucleation along the dislocation in Ti this also imposes the undesirable condition that the habit plane of the nucleus contains the chosen line direction. However, there is no *a priori* reason to expect the elastically preferred habit plane to be perpendicular to the $\langle 1\ 1\ 1 \rangle_\beta$ family of directions, and in fact there is evidence to suggest that it is not.

Kashchenko and Chashchina predicted from elasticity theory that for pure Ti this habit plane should be $\{\bar{1}\ 1.5356\ \bar{1}\}_\beta$[45], and Morris *et al.* made a similar prediction in a titanium alloy[46]. This habit plane normal is clearly not perpendicular to the dislocation line direction $[1\ 1\ 1]_\beta$, unlike the $\{\bar{1}\ 2\ \bar{1}\}_\beta$ habit plane observed in the few-layer simulations.

In the many-layer supercells, as in the few-layer supercells, the precipitates are plate-like and begin with $\{\bar{1}\ 2\ \bar{1}\}_\beta$ type habit planes (see Figure 7a). However, in the longer cells most of these plates change growth direction to alter the habit plane during growth of the supercritical nuclei, gliding portions of the dislocations with them (as done by one of the plates in Figure 8). This shifts the habit plane from $\{\bar{1}\ 2\ \bar{1}\}_\beta$ to approximately $\{\bar{1}\ 1.61\ \bar{1}\}_\beta$ before the transformation proceeds too far to allow habit plane identification. This rotation is towards the direction predicted by elasticity theory calculations[45,46], but still limited by the periodic boundary conditions. Because the dislocation line must be periodic, a section of it glides to connect the twisted line to its image (see Figure 8b), and the energy associated with this increase in line length resists the rotation caused by the precipitate. At the slipped segment the precipitate detaches from the dislocation line, forming a curved edge. We anticipate that if the supercell were infinitely long the precipitate would rotate all the way into the habit plane predicted by elasticity theory.

C. Post-Transformation Microstructure

After the transformation is complete the resulting microstructure is necessarily nano-grained, due to the supercell size. In our few-layer simulations all primary α grains have the orientation relationship $[1\ 1\ 1]_\beta \parallel [1\ 1\ \bar{2}\ 0]_\alpha$ maintained along the short axis of the supercell parallel to the dislocation line. Initially many secondary α grains are nucleated, and a very small fraction of these do not share this orientation relation (see "Other" data in Figure 5). However, during growth all of those without this relationship eventually are consumed by grains of the three dominant variants (V4, V8, V12). Further, many grains of these dominant variants are also consumed by others during coarsening after the transformation to α is complete.

We characterize boundaries between different grains by the angle between c-axes ($[0\ 0\ 0\ 1]_\alpha$ directions) in the adjacent grains and the angle the grain boundary makes with both c-axes. Due to the constrained supercell geometry, all rotations are about the $[1\ 1\ \bar{2}\ 0]_\alpha$ axis. We

find only three distinguishable orientations of the basal plane and five grain boundary types in the few-layer supercells, which we will describe in descending order of occurrence.

The most common boundary (type 1) has $[0\ 0\ 0\ 1]_\alpha$ directions at an angle of $\frac{\pi}{3}$, with the boundary at $\frac{\pi}{6}$ to each, and the boundary is a plane of mirror symmetry. This finding is consistent with previous experiment[6,11] and phase field simulations[12]. Type 2 is a boundary (stacking fault) at which the hcp stacking changes (ABA|B|CBC). In this type there is no difference in angle between the $[0\ 0\ 0\ 1]_\alpha$ directions, and both $[0\ 0\ 0\ 1]_\alpha$ directions make an angle of $\frac{\pi}{2}$ with the grain boundary. These appear as green lines in the PTM images due to the local structure in the boundary layer being identified as fcc. Type 3 boundaries have c-axes at $\frac{\pi}{3}$ as in type 1, but the boundary itself is perpendicular with the c-axis on one side of the boundary. Type 3 boundaries are asymmetric and tend to be shorter and broader (i.e. more atoms are identified as in the boundary rather than either of the neighboring grains), indicating that its energy is somewhat higher than the previous two types. The last two observed grain boundaries are much less common than the first three. In type 4 the c-axes meet at a $\frac{2\pi}{3}$ angle, with the grain boundary at $\frac{\pi}{3}$ to each. In type 5, the adjacent grains differ by stacking rather than angle as in type 2, but both c-axes meet the grain boundary at a $\frac{\pi}{6}$ angle.

Examining the simulation trajectories during the grain growth stage, we see that the commonly-observed type 1 grain boundaries often form when a new grain nucleates only a few atomic spacings from an existing α grain (see Figure 3b,c). This nucleation is apparently accommodated by the stress in the β grain resulting from the nearby α-β interface. Further, it is common to see two nearby α grains with $\frac{\pi}{3}$ difference in orientation induce the nucleation of a grain oriented to form $\frac{\pi}{3}$ angles with both (see Figure 3d). This results in structures similar to the tents seen by Balachandran *et al.* in EBSD[11] as well as Qiu *et al.* in in phase field simulations[12].

After coarsening is complete typically only type 1 boundaries between distinguishable orientations, type 2 boundaries (stacking faults) within grains, and some geometrically-necessary type 5 boundaries which connect the type 2 stacking faults remain. In many cases coarsening results in only two large grains surviving (see Figure 3f), while as many as 30 grains might exist at some point during a simulaition.

In the many-layer supercells when the transformation is near completion the same types of grain boundaries are observed as in the few-layer supercells (see Figure 7b), with a similar

columnar structure. Again the dominant boundary is the symmetric type 1 and the type 2 is the next most common. A large triple junction of symmetric $\frac{\pi}{3}$ boundaries has been observed to form when two grains grow into each other and induce a third grain to nucleate, as similarly observed in the short supercells. This in some cases creates tent-like structures formed when these three grains grow inwards toward the triple junction, a process shown in Figure 9. Nearly all grain boundaries are parallel to the original dislocation line direction, though type 2 boundaries are formed at a $\frac{\pi}{3}$ angle to the dominant grain boundary direction towards the end of the grain growth process.

V. CONCLUSION

We examined nucleation of the β to α phase transition at $\langle 1\ 1\ 1\rangle_\beta$-type screw dislocations in pure titanium through a combination of molecular dynamics simulation using a modified embedded atom method potential and elasticity theory analysis. Both methods predict the same three α variants and preferential directions for α nucleus growth in the early stages of transformation, corresponding to orientations spaced uniformly about the $\langle 1\ 1\ 1\rangle_\beta$ axis at angles $\theta = \frac{\pi}{2}$, $\theta = \frac{7\pi}{6}$, and $\theta = \frac{11\pi}{6}$ from the $\langle \bar{2}\ 1\ 1\rangle_\beta$ axis perpendicular to the dislocation. These directions are preferred because the strain field resulting from the dislocation aligns best with the transformation strain required for the Burgers path that takes the β phase to the α phase and result in habit planes that contain the dislocation line.

We have demonstrated the tendency of the α precipitate to rotate towards the elastically preferred habit plane when the simulation supercell is large enough to accommodate such a rotation. This rotation is still apparently resisted by lengthening of the remaining dislocation, to which the α precipitate remains bound by a favorable surface energy term. Finally, we examine the post-transformation α microstructure and find it to be dominated by three orientation relationships between neighboring grains.

This work demonstrates the role of the strain field around $\langle 1\ 1\ 1\rangle_\beta$-type screw dislocations in providing heterogeneous nucleation sites for the α phase, and thus provides a link between initial dislocation density in the β phase and post-transformation microstructure that could prove useful to the engineering of titanium alloys. These findings match those from experimental and phase-field simulation literature on the same system. In addition, these findings extend those deduced from phase-field simulations by enabling the time scales asso-

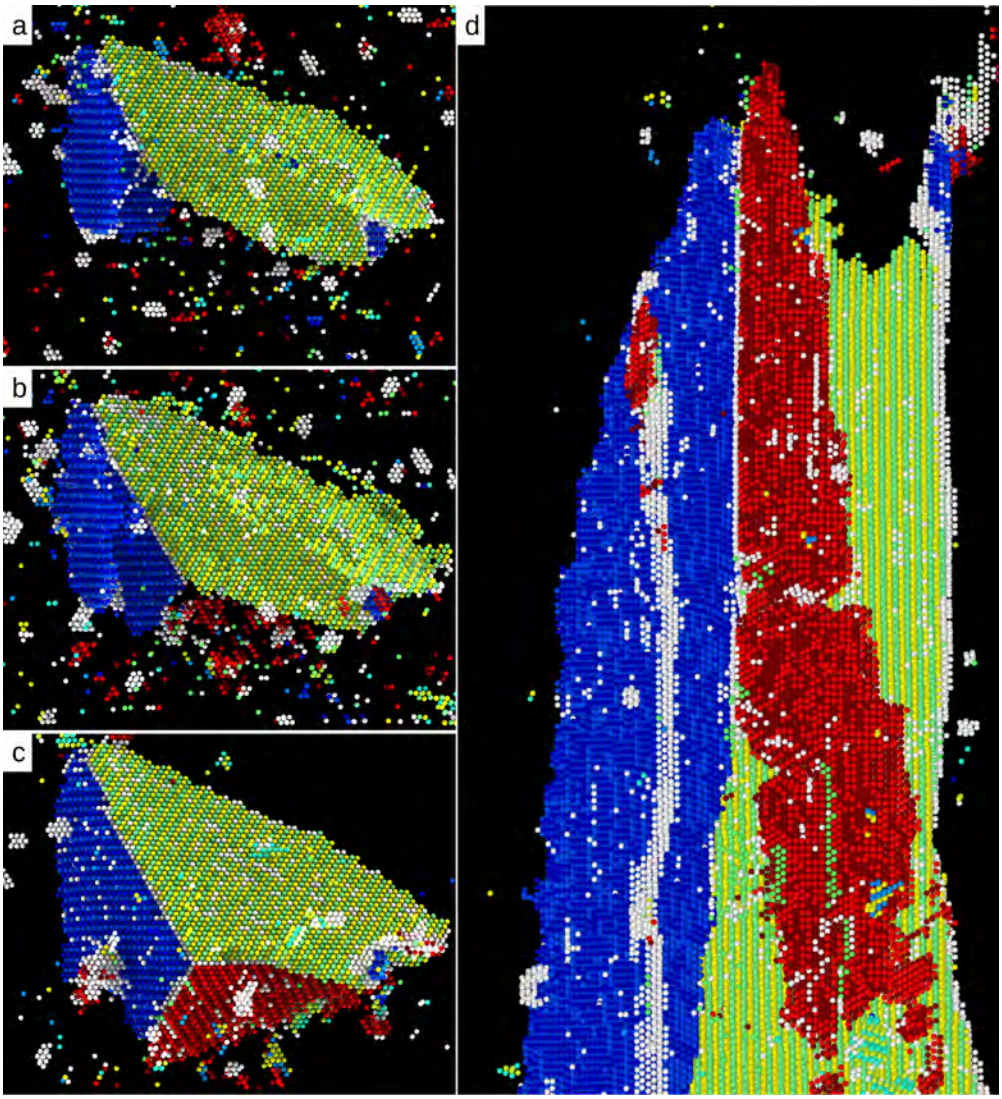

FIG. 9. Sections showing growth of two grains of the α-phase from β (atoms removed) which nucleated on dislocation lines in the supercell which is 737 Å in length. Atom coloring is by PTM as described previously. (a) The two original grains growing from the dislocations with $\frac{2\pi}{3}$ orientation difference have intersected and formed a type 1 grain boundary. (b) The nucleation of a third grain with complementary orientation is induced by the strain around the original two grains. (c) The three grains have grown until they form a tent structure with three type 1 grain boundaries. (d) Side view of the same structure, without sectioning. This clearly shows the tent shape of the colony.

ciated with nucleation to be explored directly. Within molecular dynamics simulations, the processes determining nucleation rates are allowed to evolve at the atomic scale. Moreover,

the molecular dynamics simulations allow for the motion of the dislocation that accommodates the habit plane shift after nucleation. This demonstrates the potential of molecular dynamics simulations for studying variant selection in solid/solid phase transitions.

VI. ACKNOWLEDGEMENTS

The authors acknowledge helpful discussions with Professor Dallas Trinkle about the MEAM potential for titanium used in the simulations presented, as well as with Dr. Rodrigo Freitas and Prof. Mark Asta about the thermodynamic integration method. M. Poschmann, J. Lin, and D. C. Chrzan gratefully acknowledge funding from the U.S. Office of Naval Research under grant N00014-16-1-2304. This research used the Savio computational cluster resource provided by the Berkeley Research Computing program at the University of California, Berkeley (supported by the UC Berkeley Chancellor, Vice Chancellor for Research, and Chief Information Officer). I. S. Winter gratefully acknowledges funding from the U.S. Office of Naval Research under grant N00014-16-1-3124.

---

* maxp@berkeley.edu, dcchrzan@berkeley.edu

[1] W G Burgers, "On the Process of Transition of the Cubic-Body-Centered Modification into the Hexagonal-Close-Packed Modification of Zirconium," (1933).

[2] N. Gey, M. Humbert, M.J. Philippe, and Y. Combres, "Investigation of the α- and β- texture evolution of hot rolled Ti-64 products," Materials Science and Engineering: A **219**, 80–88 (1996).

[3] N Gey, M Humbert, M.J. Philippe, and Y Combres, "Modeling the transformation texture of Ti-64 sheets after rolling in the β-field," Materials Science and Engineering: A **230**, 68–74 (1997).

[4] Z.S Zhu, J.L Gu, R.Y Liu, N.P Chen, and M.G Yan, "Variant selection and its effect on phase transformation textures in cold rolled titanium sheet," Materials Science and Engineering: A **280**, 199–203 (2000).

[5] N. Gey and M. Humbert, "Characterization of the variant selection occurring during the $\alpha \rightarrow \beta \rightarrow \alpha$ phase transformations of a cold rolled titanium sheet," Acta Materialia **50**, 277–287 (2002).

[6] S.C. Wang, M. Aindow, and M.J. Starink, "Effect of self-accommodation on α/α boundary populations in pure titanium," Acta Materialia **51**, 2485–2503 (2003).

[7] D. Bhattacharyya, G.B Viswanathan, Robb Denkenberger, D. Furrer, and Hamish L. Fraser, "The role of crystallographic and geometrical relationships between α and β phases in an α/β titanium alloy," Acta Materialia **51**, 4679–4691 (2003).

[8] I. Lonardelli, N. Gey, H.-R. Wenk, M. Humbert, S.C. Vogel, and L. Lutterotti, "In situ observation of texture evolution during $\alpha \rightarrow \beta$ and $\beta \rightarrow \alpha$ phase transformations in titanium alloys investigated by neutron diffraction," Acta Materialia **55**, 5718–5727 (2007).

[9] S.M.C. van Bohemen, A. Kamp, R.H. Petrov, L.A.I. Kestens, and J. Sietsma, "Nucleation and variant selection of secondary α plates in a β Ti alloy," Acta Materialia **56**, 5907–5914 (2008).

[10] M.R. Daymond, R.A. Holt, S. Cai, P. Mosbrucker, and S.C. Vogel, "Texture inheritance and variant selection through an hcp–bcc–hcp phase transformation," Acta Materialia **58**, 4053–4066 (2010).

[11] Shanoob Balachandran, Ankush Kashiwar, Abhik Choudhury, Dipankar Banerjee, Rongpei Shi, and Yunzhi Wang, "On variant distribution and coarsening behavior of the α phase in a metastable β titanium alloy," Acta Materialia **106**, 374–387 (2016).

[12] D. Qiu, R. Shi, D. Zhang, W. Lu, and Y. Wang, "Variant selection by dislocations during α precipitation in α/β titanium alloys," Acta Materialia **88**, 218–231 (2015).

[13] D. Qiu, R. Shi, P. Zhao, D. Zhang, W. Lu, and Y. Wang, "Effect of low-angle grain boundaries on morphology and variant selection of grain boundary allotriomorphs and Widmanstätten side-plates," Acta Materialia **112**, 347–360 (2016).

[14] R. Shi, N. Zhou, S.R. Niezgoda, and Y. Wang, "Microstructure and transformation texture evolution during α precipitation in polycrystalline α/β titanium alloys – A simulation study," Acta Materialia **94**, 224–243 (2015).

[15] Steve Plimpton, "Fast Parallel Algorithms for Short-Range Molecular Dynamics," Journal of Computational Physics **117**, 1–19 (1995).

[16] R. G. Hennig, T. J. Lenosky, D. R. Trinkle, S. P. Rudin, and J. W. Wilkins, "Classical potential describes martensitic phase transformations between the α, β, and ω titanium phases," Physical

Review B **78**, 054121 (2008), arXiv:0706.1764.

[17] Rodrigo Freitas, Mark Asta, and Maurice De Koning, "Nonequilibrium free-energy calculation of solids using LAMMPS," Computational Materials Science **112**, 333–341 (2016).

[18] Daan Frenkel and Anthony J. C. Ladd, "New Monte Carlo method to compute the free energy of arbitrary solids. Application to the fcc and hcp phases of hard spheres," The Journal of Chemical Physics **81**, 3188–3193 (1984).

[19] M. de Koning, A. Antonelli, and S. Yip, "Optimized Free-Energy Evaluation Using a Single Reversible-Scaling Simulation," Physical Review Letters **83**, 3973 (1999), arXiv:9604005 [quant-ph].

[20] Maurice de Koning, Alex Antonelli, and Sidney Yip, "Single-simulation determination of phase boundaries: A dynamic Clausius–Clapeyron integration method," The Journal of Chemical Physics **115**, 11025–11035 (2001).

[21] D Dickel, C D Barrett, R L Carino, M I Baskes, and M F Horstemeyer, "Mechanical instabilities in the modeling of phase transitions of titanium," Modelling and Simulation in Materials Science and Engineering **26**, 065002 (2018).

[22] W. Petry, A. Heiming, J. Trampenau, M. Alba, C. Herzig, H. R. Schober, and G. Vogl, "Phonon dispersion of the bcc phase of group-iv metals. i. bcc titanium," Phys. Rev. B **43**, 10933–10947 (1991).

[23] Murray S. Daw, "Elasticity effects in electronic structure calculations with periodic boundary conditions," Computational Materials Science **38**, 293–297 (2006).

[24] Niklas Lehto and Sven Öberg, "Effects of Dislocation Interactions: Application to the Period-Doubled Core of the 90° Partial in Silicon," Physical Review Letters **80**, 5568–5571 (1998).

[25] Seungwu Han, Luis A. Zepeda-Ruiz, Graeme J. Ackland, Roberto Car, and David J. Srolovitz, "Interatomic potential for vanadium suitable for radiation damage simulations," Journal of Applied Physics **93**, 3328–3335 (2003).

[26] Alexander Stukowski, "Visualization and analysis of atomistic simulation data with OVITO – the Open Visualization Tool," Modelling and Simulation in Materials Science and Engineering **18**, 015012 (2010).

[27] Peter Mahler Larsen, SØren Schmidt, and Jakob SchiØtz, "Robust structural identification via polyhedral template matching," Modelling and Simulation in Materials Science and Engineering **24** (2016), 10.1088/0965-0393/24/5/055007, arXiv:1603.05143.

[28] Aidan P Thompson, Steven J Plimpton, William Mattson, Aidan P Thompson, Steven J Plimpton, and William Mattson, "General formulation of pressure and stress tensor for arbitrary many-body interaction potentials under periodic boundary conditions," **154107** (2013), 10.1063/1.3245303.

[29] Daan Frenkel and Berend Smit, Understanding molecular simulation: from algorithms to applications, Vol. 1 (Academic press, 2001) pp. 519–523.

[30] MEJ Newman and GT Barkema, Monte Carlo Methods in Statistical Physics (Oxford University Press: New York, USA, 1999) pp. 69–70.

[31] Hirotsugu Ogi, Satoshi Kai, Hassel Ledbetter, Ryuichi Tarumi, Masahiko Hirao, and Kazuki Takashima, "Titanium's high-temperature elastic constants through the hcp-bcc phase transformation," Acta Materialia **52**, 2075–2080 (2004).

[32] E.S. Fisher and D. Dever, "The single crystal elastic moduli of beta-titanium and titanium–chromium alloys," in The Science, Technology and Application of Titanium, edited by R.I. Jaffee and N.E. Promisel (Pergamon, 1970) pp. 373 – 381.

[33] Massel Ledbetter, Hirotsugu Ogi, Satoshi Kai, Sudook Kim, and Masahiko Hirao, "Elastic constants of body-centered-cubic titanium monocrystals," Journal of Applied Physics **95**, 4642–4644 (2004).

[34] J. W. Cahn, "Nucleation on dislocations," Acta Metallurgica **5**, 169 – 172 (1957).

[35] G. Thomas and J. Nutting, "The mechanism of phase transformations in metals," Institute of Metals, London , 57–66 (1956).

[36] A. Kelly and R. B. Nicholson, "Precipitation hardening," Progress in Materials Science **10**, 151 – 391 (1963).

[37] DJ Bacon, DM Barnett, and Ronald Otto Scattergood, "Anisotropic continuum theory of lattice defects," Progress in Materials Science **23**, 51–262 (1980).

[38] D. C. Chrzan, M. P. Sherburne, Y. Hanlumyuang, T. Li, and J. W. Morris, "Spreading of dislocation cores in elastically anisotropic body-centered-cubic materials: The case of gum metal," Phys. Rev. B **82**, 184202 (2010).

[39] T Furuhara, S Takagi, H Watanabe, and T Maki, "Crystallography of grain boundary α precipitates in a β titanium alloy," Metallurgical and Materials Transactions A **27**, 1635–1646 (1996).

[40] Doyl Dickel, Christopher D Barrett, Ricolindo L Carino, Michael I Baskes, and Mark F Horstemeyer, "Mechanical Instabilities in the Modeling of Phase Transitions of Titanium," Modelling and Simulation in Materials Science and Engineering , 0–22 (2018).

[41] Melvin Avrami, "Kinetics of phase change. i general theory," The Journal of Chemical Physics **7**, 1103–1112 (1939), https://doi.org/10.1063/1.1750380.

[42] Melvin Avrami, "Kinetics of phase change. ii transformation-time relations for random distribution of nuclei," The Journal of Chemical Physics **8**, 212–224 (1940), https://doi.org/10.1063/1.1750631.

[43] Melvin Avrami, "Granulation, phase change, and microstructure kinetics of phase change. iii," The Journal of Chemical Physics **9**, 177–184 (1941), https://doi.org/10.1063/1.1750872.

[44] The full trajectory data is available via the UC Berkeley Library Dash project under the same title as this article (or at https://doi.org/10.6078/D1QS94). The authors recommend interested readers visualize the data using OVITO and applying the polyhedral template matching modification, as we have done to generate our figures.

[45] M. P. Kashchenko and V. G. Chashchina, "Crystal dynamics of the BCC-HCP martensitic transformation: I. Controlling wave process," The Physics of Metals and Metallography **105**, 537–543 (2008).

[46] J. W. Morris, Y. Hanlumyuang, M. Sherburne, E. Withey, D. C. Chrzan, S. Kuramoto, Y. Hayashi, and M. Hara, "Anomalous transformation-induced deformation in ⟨1 1 0⟩ textured Gum Metal," Acta Materialia **58**, 3271–3280 (2010).